Anti-clogging ability of the labyrinth emitter and its evaluation method

Wenqian Zhang[1,2], Zhaoxi Wang[1,2], Senhao Cheng[1,2], Aihong Dong[1,2],
Erxin Zhang[1,2], Wenquan Niu[3,4*]

(1. *Key Laboratory of Agricultural Soil and Water Engineering in Arid and Semiarid Areas, Ministry of Education,*
Northwest A&F University, Yangling 712100, Shaanxi, China;
2. *College of Water Resources and Architectural Engineering, Northwest A&F University, Yangling 712100, Shaanxi, China;*
3. *Institute of Soil and Water Conservation, Chinese Academy of Science and Ministry of Water Resources of the People's Republic of China,*
Yangling 712100, Shaanxi, China;
4. *Institute of Soil and Water Conservation, Northwest A&F University, Yangling 712100, Shaanxi, China)*

Abstract: Emitter clogging is one of the most serious factors that restrict the drip irrigation system operation and water use efficiency.   To scientifically characterize and evaluate emitter clogging risk, a literature review, short-period emitter anti-clogging tests, and CFD (Computational Fluid Dynamics) hydraulic performance tests were conducted.   Results showed that the emitter anti-clogging ability is related to its structure, material, and processing technology, not external factors.   This was evidenced in the irrigation tests, as with the different water qualities, the same emitters were repeatedly prone to clog or to avoid clogging.   A predictive model of structural resistance coefficient (Cs), a quantitative indicator of the emitter anti-clogging ability, whose value ranges between 0 and 1, was utilized.   Larger Cs values indicate a lower anti-clogging ability and thus a higher risk of clogging.   A good linear relationship between Cs and the relative flow rate was detected, and the Cs relationship with the fluidity index (x) was determined to be a power function.   The Cs should be controlled within the range of 0.146-0.461 when designing new emitters to ensure that they have good anti-clogging properties.   This research will provide theoretical guidance for the anti-clogging management of drip irrigation systems and for the design of optimal emitter structures.
Keywords: drip irrigation system, structural resistance coefficient, emitter clogging risk, energy loss, anti-clogging ability
DOI: 10.25165/j.ijabe.20221506.6781

1   Introduction

As a modern water-saving technology, drip irrigation significantly improves water use efficiency and increases grain yield and quality[1-6].   It is thus a promising tool to solve existing agricultural water shortage issues.   However, emitter clogging has consistently been the biggest obstacle in the development and large-scale application of drip irrigation systems.   Once the emitter is clogged, the irrigation system quality decreases, shortening the life of the system[7].   Local emitter clogging increases the flow rate of the unplugged emitter, resulting in an uneven distribution of water and nutrients in the soil, reducing both water use and irrigation efficiencies, lowering the yield and quality of crops[8-12].

Emitter clogging is common in drip irrigation systems and results from complex processes involving physical, chemical,

biological, and comprehensive factors.   Generally, although emitter clogging occurs via a gradual accumulation process, sudden clogging events can also occur.   However, clogging occurs after drip irrigation systems have run for a certain amount of time, and it is an inevitable end-state of the drip irrigation system.   The emitter flow rate is one of the main parameters that characterize the degree to which clogging occurs.   Some scholars[13,14] have stated that the relative flow rate (Dra) could be used to characterize the flow rate drop of a single emitter and the degree of emitter clogging.   When Dra is significantly less than a specific value (generally considered to be less than 75% of the rated flow rate), the emitter is deemed clogged.   To characterize emitter clogging, both relative flow rate and irrigation uniformity have been conventionally used to evaluate emitter clogging degrees[15-18].   However, these indexes are post-evaluation indicators applied once the emitter is clogged to evaluate the degree of emitter clogging.   Currently, there are few indicators to systematically evaluate the anti-clogging performances of different kinds of emitters, and thus, evaluations of their anti-clogging abilities are only a matter of academic speculation.   To predict whether a certain emitter is prone to clog or whether there is a difference in the processes and degree of clogging at a specific stage of irrigation among different emitters, it must first be confirmed whether there is a difference in the anti-clogging ability of different labyrinth channel emitters.   During the irrigation processes in different conditions, emitters with high anti-blocking abilities showed consistent performances.   However, it is unknown if different emitters possess inherent anti-clogging abilities.

Uniform, stable, and slow outflow is an essential feature of irrigation systems, mainly achieved using a tooth-shaped labyrinth channel in the emitter, which dissipates energy and reduces pressure. The pressure in the labyrinth channel generally shows a stepwise, uniform downward trend along the flow direction. The channel inlet pressure was the greatest, and the pressure dropped to 0 after the water flowed through the entire channel and reached the outlet[19,20]. The velocity distribution along the direction of the flow path was relatively uneven. According to the flow velocity, the fluid is divided into the mainstream and non-mainstream areas. The flow velocity near the wall and the vortex center is generally small but large at the tooth tip angle. The dynamics and mutual effect of the flow velocity and pressure field result from sudden changes in the flow channel structure (such as changes to the tooth tip angle), which interfere with the fluid dynamics and result in velocity distribution changes. In these conditions, the flow might become more turbulent, generating vortices[21,22]. In this process, the relative movement between the viscous liquid particles is enhanced, increasing the internal friction; through the continuous conversion of potential pressure energy and kinetic energy, the energy of the mainstream and non-mainstream areas continuously change and gradually dissipate[23,24]. When the drip irrigation systems were watered with water containing a high concentration of suspended material, fine particles (<0.1 mm) could still be present in the water after filtration. These small particles are subjected to the combined action of external inertial forces, drag forces, and gravity. Due to the low mass of the particles, the velocity distribution of the suspended particles generally reflects the velocity of the water flow, with the former being slower than the latter[21]. In non-mainstream areas, especially in the low-speed vortex zone, the flow velocity is generally less than 0.8 m/s, with a fixed velocity dead zone (velocity is 0)[25,26]. Tiny particles are easily dragged into vortices when passing through these areas. The residence time and the number of cycles involved in the vortex increase because of their low levels of inertia. Assuming the particles' wave speed was equal to the vortex velocity, the particles would never escape this area. Furthermore, particles tend to flocculate and to deposit under the influence of the surface charge[15], the possibility of the particles escaping from the vortex is significantly reduced for their continuous circulation increases the probability of collision, dissipating kinetic energy[27,28]. Therefore, severe emitter clogging could occur in these areas after a long-time usage. Optimizing the structural parameters of the labyrinth channel could prevent clogging[29,30]. Previous studies explored the influence of the emitter structure parameters on the fluid flow characteristics in the emitter channel and the emitter clogging by the particle image velocimetry (PIV) test, computational fluid dynamics (CFD) simulations, or a combination of both. For example, Adin and Sacks[31] conducted a field experiment and found that emitter clogging was closely related to flow channel structure. They proposed methods such as shortening the flow channel length, widening the flow channel width, and dulling the tooth tip angle to improve anti-clogging performances. Zhang et al.[32] used CFD to calculate the passage rate of particles in the flow channel, analyzed the qualitative relationship between the passage rate of particles and the key parameters of the labyrinth channel, and performed a regression analysis to obtain a parameterized model. Yu et al.[33] combined computational fluid dynamics-digital elevation model (CFD-DEM) technology with particle tracking velocimetry (PTV) to explore

and verify the hydraulic performance and anti-clogging performance of the labyrinth channel with tooth tip angles of 30°, 45°, 60°, and 90°. A tooth tip angle in the flow channel in the range of 60°-90° is recommended to alleviate clogging. Feng et al.[34] suggested the vortex flushing wall design method to optimize the fluid path and identify the best boundary optimization strategy to maintain a balance between the hydraulic performance and the anti-clogging performance of the emitter. However, there has been limited research on how to characterize and measure the anti-clogging performance of the emitter. Current research has provided qualitative guidance on emitter optimization rather than quantitative research on the risk of emitter clogging.

Based on previous research, it was found that the tooth-shaped labyrinth flow channel emitter has an inherent anti-clogging ability, utterly independent of the quality of irrigation water, operation mode, or environmental factors. It is only related to the structure and composition of the tooth-shaped labyrinth channel, such as the channel size, material, and processing precision. As emitters from all manufacturers are constructed with polyethylene (PE) material, and the processing precision is difficult to obtain for commercial manufacturers, investigations often focus on the impact of the channel size of the emitter on anti-clogging performance[35-37]. Just as the value of commodities in economics can be reflected by price, the anti-clogging ability of drip irrigation systems can be characterized by their clogging risks. Drip irrigation systems have a smaller risk of clogging when the emitter's anti-clogging ability is high, and vice versa. This research selected three different water qualities, using a combination of short-period blockage tests, CFD simulation tests, and a literature review to identify if the anti-clogging ability of the emitter is an inherent property. Supported by the energy loss principle, an evaluation model for the anti-clogging ability of the emitters was initially constructed and the clogging risks of different emitters were evaluated and verified. This research could provide a theoretical basis for the selection of suitable emitters.

2 Materials and methods

2.1 Anti-clogging test

2.1.1 Experimental materials
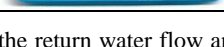
Sediment was collected from the riverbed of the Qingtongxia floodplain of the Yellow River, in the Ningxia region of China, on April 23, 2018. After removing the impurities like branches and pebbles from the surface of the silt of the riverbed, a shovel was used to collect the surface silt at a depth of 0-15 cm. Collected samples were then mixed uniformly, air-dried for one month, ground into visible powder, and finally passed through a 0.1 mm screen to obtain sediments of the target diameter. The particle size composition was measured by an APA 2000 laser particle analyzer (Malvern Panalytical, Malvern, UK). The initial particle size gradation of the sediment was as follows: 0.05-0.1 mm (24.86%), 0.02-0.05 mm (43.65%), 0.01-0.02 (3.52%), 0.005-0.01 (4.67%), 0.002-0.005 (3.27%), and <0.002 (10.02%). The mineral composition of the sediment was tested by XRD-Rietveld technology. It included quartz, plagioclase, microline, calcite, dolomite, mica, chlorite, and amphibole, which accounted for approximately 43%, 15%, 7%, 8%, 3%, 11%, 9%, and 4% of the total, respectively.

Compared with other types of emitters, toothed labyrinth flow channel emitters have shorter flow channel lengths, a compact structure, and a lower cost. Consequently, they have become one of the most popular emitters used in drip irrigation systems[32]. In

the present study, seven types of inner insert labyrinth channel emitters were entrusted to Shandong Chunyu Drip Irrigation Technology Co., Ltd. for engraving and processing.   The emitter

parameters are shown in Table 1.   The lateral diameter was 16 mm, wall thickness was 0.38 mm, and the distance between the emitters was 30 cm or 50 cm.

Table 1   Structural parameters of the seven experimental emitters

No.	Tooth width $/\times10^{-3}$ m	Tooth height $/\times10^{-3}$ m	Tooth spacing $/\times10^{-3}$ m	Channel width $/\times10^{-3}$ m	Channel dept $/\times10^{-3}$ m	Number of channel units	Flow regime index (x)	Flow coefficient (k)	Structure of emitter
E1	1.50	1.50	3.04	1.25	1.25	8	0.44	0.50	
E2	1.50	1.50	2.74	1.00	1.00	8	0.47	0.50	
E3	1.50	1.80	2.88	1.00	1.00	12	0.50	0.42	
E4	1.50	1.00	2.25	0.75	0.75	10	0.48	0.30	
E5	0.60	1.00	2.46	1.25	1.25	12	0.50	0.38	
E6	0.60	1.80	1.87	0.75	0.75	8	0.46	0.32	
E7	1.80	1.00	3.04	1.25	1.25	10	0.48	0.55	

2.1.2   Experimental device

The anti-clogging test platform was built with reference to the Agricultural Irrigation equipment - Emitters and emitter pipe - Specification and test methods (GB/T 17187-2009), Micro-irrigation emitters - micro tubings, micro tapes (SL/T 67.2-1994) and Clogging test methods for emitters (ISO/TC 23/SC 18/WG5 N4).   The test platform included water source preparation, water supply system, control device, drip irrigation laterals to be tested, and drainage device (Figure 1).   The first part was equipped with two buckets, of which one was used to prepare the water source and the other to ensure a continuous water supply to the system.   Both buckets were equipped with mixers to ensure uniform distribution and a stable concentration of particles in the water source and eliminate sedimentation during irrigation process.   A pressure sensor (OHR-M2 pressure transducer, Hongrun Precise Instrument Company) was installed to monitor the working pressure in real time.   The operating system was adjusted to incorporate an electric ball valve that could control the degree to

which was open, so that it could adjust the return water flow and maintain a stable working pressure.   The pressure control error was less than 1.25%.   At the same time, the opening and closing time of the mixer and the water pump were controlled to achieve the expected irrigation time.   A total of 5 laterals were laid on the test platform.   The system was automatically cleaned to reduce the interference of the system's silt and sand on the test results after one group test.

2.1.3   Experiment design and implementation

In this experiment, three suspended particle concentrations of 0.5 g/L, 1.5 g/L, and 3.0 g/L were set.   The test was carried out from July 4th, 2019, to October 16th, 2019.   The anti-clogging test was designed with reference to the draft international drip irrigation emitter anti-clogging performance test standard.   The drip irrigation system was run for 8 irrigation events per day.   Each irrigation lasted for 1 h followed by a 30 min break.   In total, 40 irrigation events were performed for each treatment.   When the suspended particle concentration was 3.0 g/L, the flow rate sharply decreased.   Therefore, the test ended early in 20 irrigation events. Each emitter was tested 4 times.   The flow rate testing time was 30 min after the running pressure (100 kPa) stabilized.

2.2   Numerical simulation

2.2.1   Simulation principle

CFD refers to analyzing physical phenomena, such as fluid flow and heat conduction, by numerical calculations and visualization.   The application of CFD replaces the continuous fields of physical quantities in the time and space domains, such as velocity and pressure, with a set of variable values at a series of finite discrete points.   A set of algebraic equations that describe the relationship between field variables at these discrete points is established using different principles and methods, and then the algebraic equation set is solved to obtain an approximate value for the field variables.   In the field of fluid mechanics, CFD can be regarded as a numerical simulation of flow under the control of the basic flow equations (mass conservation equation, momentum conservation equation, and energy conservation equation).   The distribution of the basic physical quantities (such as speed, pressure, temperature, and concentration) at various positions in the flow field of some extremely complex problems and the changes in these physical quantities over time can be inferred through numerical simulations.   Then the vortex distribution characteristics, cavitation characteristics, and outflow zone are determined.   Other related physical quantities, such as rotary torque, hydraulic loss,
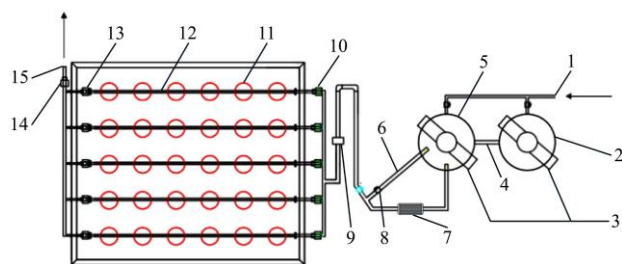
a. Schematic diagram of testing device

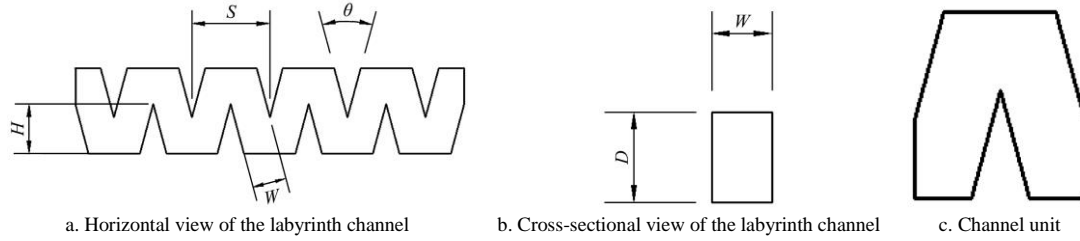b. Real platform during the testing process.

1. Water inlet pipe 2. Water preparation bucket 3. Mixer 4. Connecting pipe 5. Water supply bucket 6. Backwater pipe 7. Water pump 8. Backwater control valve 9. Flow meter 10. Electromagnetic valve 11. Weighing device 12. Laterals 13. Shut-off pumps 14. Drainage valve 15. Drainage pipe

Figure 1   Diagram of the anti-clogging test device

and fluid machinery efficiency. Its application in the emitter structure design accelerates the development and design of emitters by realizing the rapid manufacturing potential of emitter molds, which shortens the design time and reduces development cost. In this investigation, Fluent 6.0 (Fluent software company, USA) was applied to the realization of CFD.

2.2.2 Parameter selection and experimental design

The triangular tooth-shaped labyrinth channel structure was defined by the channel width (W), channel depth (D), tooth height (H), tooth tip angle (θ), tooth spacing (S), and the number of channel units (n) (Figure 2). The specific structural parameters are shown in Table 2.

a. Horizontal view of the labyrinth channel   b. Cross-sectional view of the labyrinth channel   c. Channel unit

Note: θ-tooth tip angle, (˚); D-channel depth, m; H-tooth height, m; S-tooth spacing, m; W-channel width, m.

Figure 2   Detailed size and structure of the labyrinth channel

Table 2   Parameter design for the simulated emitters

Level	Parameters					
	Tooth tip angle θ	Channel depth D ($\times 10^{-3}$ m)	Tooth height H ($\times 10^{-3}$ m)	Tooth spacing S ($\times 10^{-3}$ m)	Channel width W ($\times 10^{-3}$ m)	Number of channel units n
1	$\pi/6$	0.7	1.7	2.4	0.7	8
2	$\pi/3$	0.8	2.0	2.7	0.8	12
3	$\pi/2$	0.9	2.3	3.0	0.9	16
4	$2\pi/3$	1.0	2.6	3.3	1.0	20

2.2.3 Calculation model and boundary conditions

(1) Control equation

The fluid inside the emitter channel was mainly water. During the numerical simulation, it was assumed that the liquid was a viscous and incompressible fluid that flowed steadily at 20 ℃, ignoring the mass force and surface tension of the fluid. The law of fluid movement conforms to the laws of mass conservation and momentum conservation. The basic governing equations are the Navier-Stokes equations[38], as follows:

Continuous equation:

$$\frac{\partial u}{\partial x} + \frac{\partial v}{\partial y} + \frac{\partial w}{\partial z} = 0 \qquad (1)$$

Navier-Stokes equations:

$$\frac{\partial(\rho u)}{\partial t} + \nabla \cdot (\rho u U) = -\frac{\partial p}{\partial x} + \mu \nabla^2 u + \rho f_x$$

$$\frac{\partial(\rho v)}{\partial t} + \nabla \cdot (\rho v U) = -\frac{\partial p}{\partial y} + \mu \nabla^2 v + \rho f_y \qquad (2)$$

$$\frac{\partial(\rho w)}{\partial t} + \nabla \cdot (\rho w U) = -\frac{\partial p}{\partial z} + \mu \nabla^2 w + \rho f_z$$

where, U is the fluid velocity, m/s; u, v, w are the components of the velocity in the x, y, z coordinate axis direction; ρ is the density of water, kg/m³; μ is the dynamic viscosity coefficient, Pa/m²; p is the pressure of the fluid, Pa; f_x, f_y, f_z is the component of the mass force in the x, y, z coordinate axis directions; and when the only mass force is gravity, $f_x = f_y = 0$, $f_z = -g$.

(2) Turbulence model

The turbulence models provided by Fluent include the zero-equation model, one equation (Spalart-Allmaras) model, k-ε double equation model (including standard k-ε model, RNG k-ε model, Realizable k-ε model), Reynolds stress (RSM) model, and large eddy simulation (LESS) model, among which the k-ε model has previously been widely used for flow field simulations of labyrinth channels because of its advantage of a fast calculation speed and wide application range. The standard k-ε model has been improved to obtain the Realizable k-ε model and the RNG k-ε model.

It is generally believed that the critical Reynolds number in a microchannel structure is less than 312[39]. The data preprocessing results of this study showed that the Reynolds number in a labyrinth channel structure under 10 mH₂O conditions was approximately 316, which can be regarded as the fluid in the labyrinth channel in a turbulent state. At 10 mH₂O pressure, the relative error between the local head loss of the standard k-ε model simulation unit and the measured value was between 0.63% and 8.86%; the errors between the calculated and measured values in the RNG k-ε model and Realizable k-ε model were in the range of 3.58%-18.91% and 21.00%-37.67%, respectively. From the perspective of the flow deviation, the standard k-ε model was the best for simulation authenticity. Therefore, this study used the standard k-ε model to calculate the hydraulic performance of the fluid in the emitter channel with different structural parameters as the basic data for the research.

(3) Wall surface treatment

Turbulence models are often used when CFD was adopted to solve fluid mechanics problems. It should be noted that the turbulence model was generally aimed at fully developed turbulence flows with high Reynolds numbers. The Reynolds number of the general near-wall area was small because of the viscosity, and the turbulence that developed was not sufficient. Therefore, the near-wall area needs special treatment instead of being processed by the turbulence model. Fluent uses the wall function method to deal with the flow in the near-wall zone. The aim is to directly use semi-empirical formulas to solve the viscous bottom layer and to apply the turbulence model to get a solution in the troposphere. The standard wall function method was chosen in this research.

(4) Calculation area, boundary conditions, and meshing

The inlet and outlet boundary conditions of the flow channel were set under pressure, and the other parts of the flow channel adopted solid wall boundary conditions. The inlet pressure values were set to 20, 40, 60, 80, 100, 120, and 140 kPa. The tests were

free outflow tests; that is, the outlet pressure value was 0 kPa.

Grids are the basis of CFD analysis, and the quality of each grid significantly influences the accuracy and efficiency of the calculation.   In this paper, a hybrid grid was selected to mesh the flow in the triangular-tooth-shaped labyrinth channel.   The meshing software included Fluent and was used to divide the model. The calculation area and grid model are shown in Figure 3.
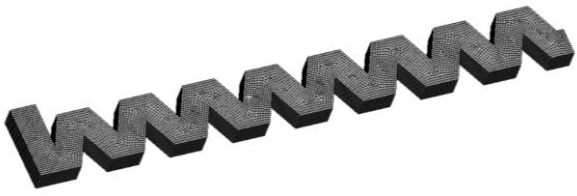

Figure 3   Grid division of the emitter flow channel unit

2.3   Literature review

Thirty-two documents related to the anti-clogging ability of emitters, published from 2010 to 2020, were identified and reviewed.   Among them, nine documents[13,18,40-46] satisfied the following three requirements.   Firstly, they described no less than two types of emitters.   Secondly, they had the same irrigation times for all emitters.   Finally, the flow rates for the emitters at the end of the irrigation were reported.   These documents were thus selected to analyze differences in clogging for different tooth-shaped labyrinth channel emitters with various water qualities, working pressures, and irrigation and flushing frequencies.   Ei-j represents the tooth-shaped labyrinth channel emitter j of case i.   The specific structure parameters of the labyrinth channel are not listed in these articles and for the details the relevant literature should be referenced.   For example, E_{8-1} represents the tooth-shaped labyrinth emitter 1 in case 8.

2.4   Data treatment

2.4.1   Hydraulic performance and anti-clogging performance

(1) Hydraulic performance

The hydraulic performance of the emitter mainly includes the flow coefficient (k) and the flow state index (x), which characterize the flow capacity and the turbulent energy dissipation capacity, respectively.   The relationship between the flow rate of the emitter and the pressure change can be expressed in the form of a power function:

$$Q = kH^x \tag{3}$$

where, Q is the flow rate, L/h; h is the pressure, kPa; k is the flow coefficient; x is the flow regime index.

Power function regression was performed on the operating pressure h and the corresponding outlet water flow Q to obtain the values of the flow coefficient k and the flow regime index x.

(2) Anti-clogging performances

The average relative flow (Dra) can characterize the overall clogging level of the entire drip irrigation pipe (lateral).   As the density of sandy water is greater than the water flow, to eliminate errors caused by the sediment, the ratio of the emitter's flow at the start and end of the irrigation system was used to characterize the average relative flow (Dra).   The temperature error was corrected using Pei's method[47].

$$Dra = \frac{\sum_{i=1}^{n} \frac{q_t}{q_i}}{N} \times 100\% \tag{4}$$

where, Dra is the average relative flow, %; q_t indicates the flow after irrigation, L/h; q_i is the flow at the initial stage of irrigation, L/h; N is the number of measured emitters on a lateral.

2.4.2   Energy index processing

The energy loss in this study was mainly the frictional head loss and local head loss caused by the fluid flowing through the labyrinth channel.

$$h_w = \lambda \frac{l}{d} \frac{v^2}{2g} + \zeta \frac{v^2}{2g} \tag{5}$$

$$v = \frac{Q}{WD} \tag{6}$$

where, h_w is the total energy loss, taking the inlet and outlet pressure differences of the 10 mH$_2$O; λ is the frictional resistance coefficient; l is the flow channel length, m; d is the flow channel diameter, m; v is the average flow velocity of the emitter cross-section; ξ is the local resistance coefficient.   Additionally, $\frac{v^2}{2g}$ is the fluid kinetic energy, m; $\lambda \frac{l}{d} \frac{v^2}{2g}$ the frictional head loss, m; and $\zeta \frac{v^2}{2g}$ is the local head loss, m.

Assuming that there is still turbulence near the wall, the Ali Tesuri formula was selected for the calculation:

$$\lambda = 0.11(\frac{\Delta}{d} + \frac{68}{Re})^{0.25} \tag{7}$$

where, Q is the flow rate of the emitter, the value of the testing emitter was obtained at 10 mH$_2$O, and the value of the simulated emitter was calculated using Fluent software, L/h; Δ is the surface roughness of the flow channel, the value is 0.0002; Re is the Reynolds number.   The cross-section of the emitter channel was rectangular, so the equivalent diameter (d) was taken as the calculated diameter here:

$$d = 2R \tag{8}$$

where, R is the fluid hydraulic radius, meter.

2.4.3   Structural resistance coefficient (Cs)

To further standardize and express the differences in the anti-clogging performance of the emitter with different structures, the local resistance coefficient (ζ) of the emitter was transformed to obtain the structural resistance coefficient (Cs), as follows:

$$Cs = \frac{\zeta - \zeta_{min}}{\zeta_{max} - \zeta_{min}} \tag{9}$$

where, Cs is the local resistance coefficient of the emitter flow channel; ζ_{min} is the minimum value, which is 19 in this investigation; ζ_{max} is the maximum value, which is 568 in this investigation.

2.4.4   Data analysis

SPSS software (IBM SPSS Statistics 23) was used to analyze the relationship between the clogging degree and the indexes for the fluid kinetic energy and the correlation analysis between the local resistance coefficient ζ and the structural parameters for seven emitters (E1, E2, E3, E4, E5, E6, E7), separately.   The quantitative relationship between the local resistance coefficient (ζ) and the structural parameters of the CFD simulating emitters was analyzed using a combination of dimensional analysis and linear regression.   The emitter structural parameters and flow rate from this research and Wen[48] were used for linear regression and compared to the three structural coefficients.   OriginPro 8 software was used to draw all figures.

3   Results and discussion

3.1   Anti-clogging ability as an inherent attribute of the emitter with labyrinth channels

3.1.1   Indoor test

Figure 4 shows the relative flow rate (Dra) of the seven labyrinth channel emitters when the concentration of the suspended particles was 0.5, 1.5, and 3.0 g/L, respectively.   As the irrigation times increased, the Dra showed a decreasing trend.   When the sand concentrations were 0.5 and 1.5 g/L, the Dra for E7 was between 96.3% and 91.0% after the 40th irrigation event.   E7 had the maximum Dra value among the 7 emitters during the entire irrigation process, while the value for E6 was always lower than the other emitters.   The Dras of E1, E2, E3, E4 and E5 were always between those of E6 and E7.   When the sand concentration was 3.0 g/L, due to the extremely high sediment concentration, most of the emitters experienced a sudden drop in the flow rate, but there was little difference among the flow drops for the seven emitters.   Like the situation when the sediment concentrations were 0.5 and 1.5 g/L, the Dra of E6 dropped sharply at the earliest stage (first irrigation) and remained the lowest value among the 7 emitters after 5 irrigation events.   The Dra of E7 maintained a uniform decrease between irrigation events 0-12.   After 12 irrigation events, the Dra of E7 shifted between sudden decreases and a slow recovery toward the maximum value identified during the irrigation process.   The Dras of E1, E2, E3, E4 and E5 dropped sharply after 3-5 irrigations and were maintained between the Dras of E6 and E7. The results show that some emitters (such as E7 in this experiment) were not easily clogged when irrigated with different water qualities, while some emitters (such as E6) appeared to always be easily clogged with the various different water qualities.   It indicates that there are different anti-clogging capabilities between the various emitters, and that the anti-clogging ability may be an inherent attribute of the emitter.
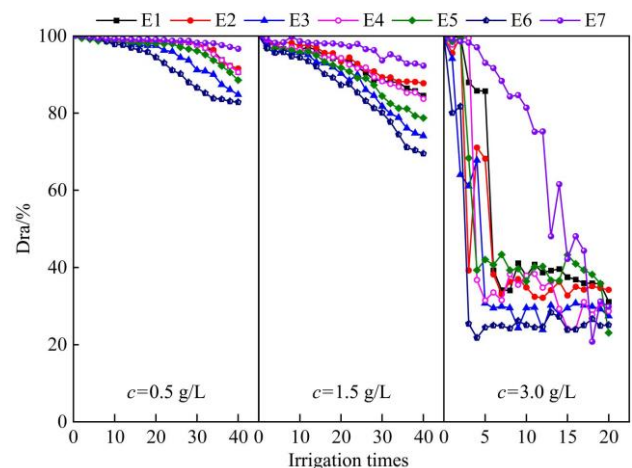

Note: 1. c=0.5 g/L, c=1.5 g/L and c=3.0 g/L represent that the sand concentrations of the irrigating water were 0.5 g/L, 1.5 g/L and 3.0 g/L, respectively.   2. E1, E2, E3, E4, E5, E6, and E7 stand for seven different emitters in Table 1.

Figure 4   The relative flow rate (Dra) of the emitters varies with irrigation times

3.1.2   Statistical analysis of the literature

Differences in clogging for different tooth-shaped labyrinth channel emitters with various water qualities, working pressures, and irrigation and flushing frequencies were analyzed from nine selected reports (Figure 5).
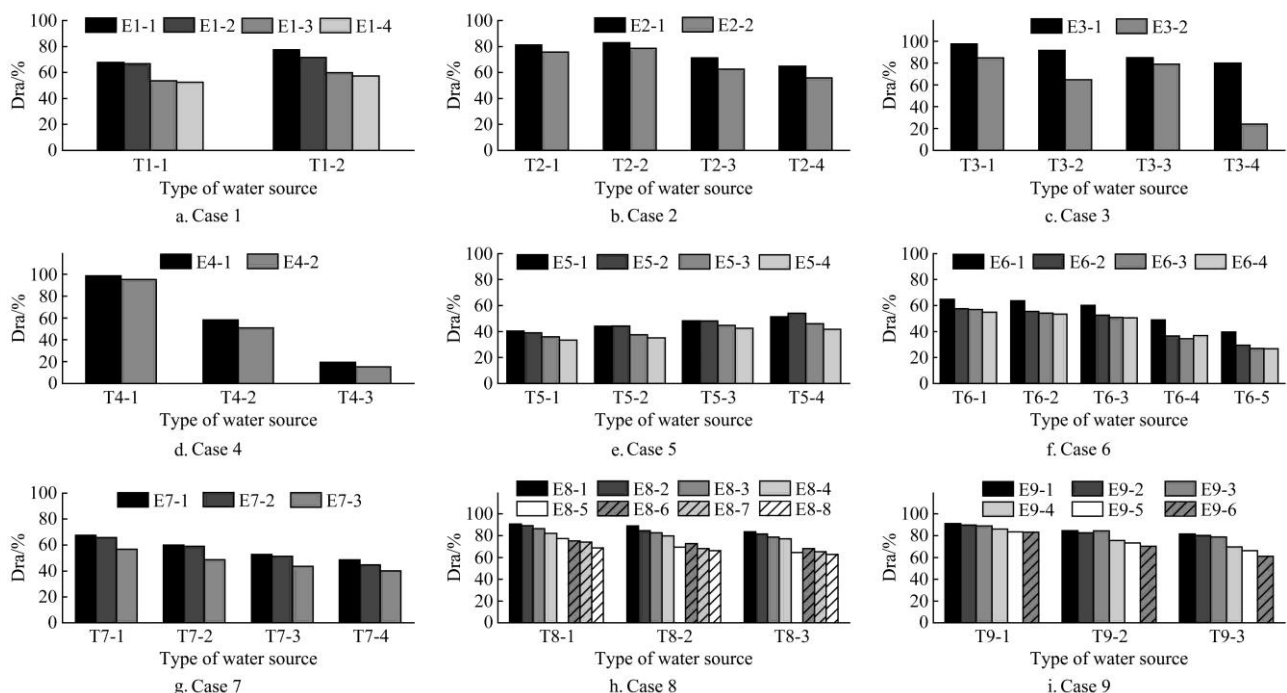
Note: 1. In the figure, Ei-j represents the tooth-shaped labyrinth channel emitter j of case i. The specific structure parameters of the labyrinth channel are not listed in these articles, and for details, the relevant literature should be referenced[13,18,40-46].   For example, E8-1 represents the tooth-shaped labyrinth emitter 1 in case 8.

Figure 5   Flow rate statistics of different emitters at the end of the irrigation treatments

Two kinds of wastewater were treated with a fluidized-bed reactor (FBR) and biological aerated filter (BAF) and then used to assess the four different emitter clogging, which showed consistent clogging results with all types of wastewater.   After 54 irrigation events, the Dra of the E1-1 with the two water types was 67.8% and 77.4%, respectively, and was always higher than that of other emitters, while the degree of clogging was always the lowest.   By contrast, the clogging of E1-4 always occurred first, and the Dra after 54 irrigation events was only 52.5% and 57.4%, respectively.

The differences in the degree of clogging (i.e., Dra) for the four types of emitters essentially remained the same, showing that emitter E1-1 had the best anti-clogging performance and E1-4 had the worst.   Therefore, the difference in clogging for different emitters was not obviously related to the irrigation water treatment (Figure 5a)[13].

With various calcium and magnesium ion contents, fertilizer solution concentrations, and water hardness (Figures 5b, 5c, and 5d), the differences in the clogging of the different emitters

essentially remained the same. For example, when the calcium and magnesium ion contents were 25 mg/L, 50 mg/L, and 100 mg/L in the reclaimed water and 50 mg/L in groundwater, emitter E2-2 was more prone to clog than emitter E2-1 with all concentrations (Figure 5b)[40]. Furthermore, when monoammonium phosphate-ammonium sulfate, monoammonium phosphate-urea, diammonium phosphate-ammonium sulfate, and diammonium phosphate-urea were respectively added to the water, and solutions set with the same fertilizer concentration, E3-2 was always more prone to clog than E3-1. At the end of the irrigation treatment, the Dra of E3-1 was always larger than that of E3-2 (Figure 5c)[41] in the four different water quality conditions. When the hardness was 0, 250 mg /L, and 500 mg /L, respectively, the anti-clogging performance of emitter E4-1 was always better than that of emitter E4-2 (Figure 5d). After 35 irrigation events, the Dra of E4-1 was 98.8%, 58.3%, and 19.3%, respectively, while the Dra of E4-2 was 95.3%, 50.9%, and 15.3%, respectively, which is smaller than that of E4-1[42]. Clogging differences for different emitters did not correlate with the chemical ion contents in the irrigation water. Some emitters seemingly possessed inherent anti-clogging properties. These emitters did not clog easily, independently of the ion type and content. In contrast, other emitters were always prone to be chemically clogged. The difference in the anti-clogging performance of the emitters with different labyrinth channels was not generally affected by the type or amount of ions in the water.

When the working pressures were constant (40 kPa) or dynamically changed (pressure range: 80-100 kPa, dynamic period: 40 s, change time respectively 1 h, 2 h, 4 h) during the drip irrigation process, E5-1 maintained the maximum Dra after 512 h under these conditions, at 40.4%, 44.1%, and 48.3% respectively. The Dra of E5-2 was slightly smaller than that of E_{5-1}, and the Dra value of the emitter E5-4 was always the smallest, at 33.3%, 35.2%, and 42.5%, respectively. With dynamic water pressure, the differences in the degree of clogging (Dra) for the four emitters were the same. E5-1 and E5-2 had better anti-clogging abilities, and E5-3 and E5-4 had poorer anti-clogging abilities[43]. Another example is when the irrigation pressures were 100, 80, 60, 40, and 20 kPa, as the Dras of the E6-1 were 64.8%, 63.7%, 60.2%, 48.9%, and 39.5%, respectively, which were the maximum values among the four different emitters, showing a high anti-clogging ability. In contrast, the E6-4 Dras were the lowest (54.9%, 53.4%, 50.5%, 36.9%, and 26.8% respectively) among the four different emitters. The Dras of E6-2 and E6-3 were between those of E6-1 and E6-4[44]. These results show that the system operating pressure does not affect clogging for different emitter types (Figures 5e and 5f).

Three different emitters (E7-1, E7-2, and E7-3) were treated with 4 different washing frequencies (washing frequency is once every 32 irrigation events, once every 64 irrigation events, once every 128 irrigation events, and not under flushing) with lateral flushing speeds of 0.4 m/s. After 600 h of irrigation, the clogging degree of E7-1 was the lowest with Dras of 67.6%, 60.0%, 52.8%, and 48.6%, respectively; E7-2 was the second most clogged with Dras of 65.8%, 58.9%, 51.3%, and 44.7%; and E7-3 was the most clogged with Dras of only 56.8% and 48.8 %, 43.6% and 40.2%[45] (Figure 5g). These results show that some emitters have good anti-clogging abilities under various washing frequencies, while others are more easily clogged under the same conditions.

When the irrigation frequencies were once every day, once every 4 d, and once every 7 d (Figure 5h), the Dras of E8-1 after 113 d of irrigation were 90.7%, 80.9%, and 83.8%, which was the lowest level of clogging among the 8 different emitters. E8-8 had the smallest Dras, 68.6%, 66.3%, and 62.7%, respectively, and was the most clogged emitter[46]. The clogging degrees of the other types of emitters were between these two. The Dras of the E8-5, E8-6, and E8-7 emitters had small differences, indicating that there were fluctuations in the order of their clogging with the different irrigation frequencies. In the test implementing the ISA, NI4, and NI7 methods, the differences in the clogging of the three different emitters were essentially not changed (Figure 5i). With the ISA test method, the Dras from E9-1 to E9-6 were 91%, 89.8%, 88.9%, 86.1%, 83.5%, and 83.3%, respectively. When the test method was NI4, the corresponding Dra values were 84.6%, 82.6 %, 84.4%, 75.6%, 73.3%, and 70.1%, respectively. When the test method was NI7, the corresponding Dra values were 81.5%, 80.3%, 79%, 69.7%, 66.2%, and 61.1%[18]. When the six different emitters were tested with the different methods, they all showed consistent clogging differences, indicating that the irrigation frequency and test methods could not change their relative degrees of clogging.

In summary, with the different water quality treatments, working pressures, flushing frequencies, and irrigation frequencies, Dra showed the clogging consistency for different emitters. It illustrates that the emitters with different tooth-shaped labyrinth channels had different anti-clogging capabilities, which were inherent attributes. External factors such as irrigation water quality, operating pressure, flushing frequency, irrigation frequency, and testing methods did not impact the clogging. Besides, the international anti-clogging standard draft recommends a method to test the anti-clogging ability of different types of emitters by gradually increasing the size and concentration of the particles in the irrigation water using 8 steps over a short period. The recommendation also assumes that each emitter has its own anti-clogging ability properties. Therefore, the anti-clogging ability of the emitter is only related to its structure, material, and processing technology. It is necessary to further explore the evaluation index of the emitter's anti-clogging ability, as well as the clogging behavior with different water qualities, operational management methods, and environmental conditions.

3.2   Construction of the anti-clogging ability index

3.2.1   Energy loss of the emitter with the labyrinth channel

The anti-clogging ability of the emitter is related to the structure of the emitter labyrinth, the material properties, and the surface roughness caused by the processing technology. Currently, emitters are generally constructed from high molecular polyethylene resin PE materials via injection molding. Drip irrigation equipment companies generally do not provide material properties or the processing and technical parameters to protect their commercial interests. Consequently, only the structure parameters of the labyrinth channel were taken into consideration in this investigation. Generally, if the flow resistance of the water in the flow channel is small and the energy remains high, suspended particles, ions, and microorganisms will not easily adhere to the channel wall and will cause emitter clogging. Therefore, the labyrinth emitter's energy dissipation performance may be an important indicator of the emitter anti-clogging ability. Based on the assumption that the fluid is viscous and incompressible, only loss along the way and local loss were considered.

Table 3 shows that when the working pressure was 10 mH$_2$O, the values of the frictional head loss, local head loss, and frictional resistance coefficient fluctuated between 0.08-0.22 mH$_2$O, 9.80-

9.92 mH$_2$O, and 9-17 mH$_2$O, respectively, without significant differences between the different treatments.　In contrast, the local resistance coefficients fluctuated over an extensive range, from 124-520, and there were significant differences among the different emitters.　The local head loss was much greater than the frictional loss, and the statistical results showed that the frictional loss only accounted for 0.76%-2.24% of the total head loss.　Therefore, the local head loss was the main factor when analyzing the fluid energy change in the labyrinth channel, while the influence of the frictional loss could be ignored.　Pearson correlation analysis results (Table 4) showed no significant correlation between Dra and the frictional resistance coefficient, frictional head loss, and local head loss.　However, there was a significant correlation between the local resistance coefficient and Dra.　The frictional head loss was thus ignored in this investigation.

Table 3　Comparison of the local head loss and frictional head

No.	Frictional head loss /mH$_2$O	Local head loss /mH$_2$O	Frictional resistance coefficient	Local resistance coefficient	Ratio of frictional resistance coefficient to total loss
E1	0.08	9.92	9	194	0.76
E2	0.20	9.8	10	143	2.08
E3	0.08	9.92	15	439	0.80
E4	0.22	9.78	17	211	2.24
E5	0.14	9.86	17	313	1.42
E6	0.09	9.91	13	520	0.91
E7	0.16	9.84	13	124	1.63

Table 4　Correlation analysis of the fluid energy characteristic parameters and the relative flow rate (Dra)

	Frictional resistance coefficient	Local resistance coefficient	Frictional head loss	Local head loss	Dra
Frictional resistance coefficient	1	--	--	--	--
Local resistance coefficient	−0.496	1	--	--	--
Frictional head loss	0.912**	−0.758*	1	--	--
Local head loss	−0.912**	0.758*	−1.000**	1	--
Dra	0.306	−0.952**	0.602	−0.602	1

Note: * indicates that the correlation was significant ($p<0.05$); ** indicates that the correlation was very significant ($p<0.01$).

3.2.2　Construction of the structural resistance coefficient (Cs)

(1) Structural parameters and the local resistance coefficient

As shown in Figure 6, for the key independent parameters of the labyrinth channel, the local resistance coefficient (ζ) significantly correlated with their width (W) and depth (D), tooth tip angle (θ), and tooth spacing (S), respectively ($p<0.05$); for the logic parameters of the labyrinth channel, different degrees of correlation between ζ and the ratio of the tooth height-to-channel width (r_1), the minimum value of the width and height (L_{min}), as well as the number of channel units (n), were observed.　There was collinearity between the width and depth of the channel with ζ.　There was no significant correlation ($p>0.05$) between ζ and the ratio of the channel width-to-depth (r_2).　However, it is difficult to neglect the influence of the ratio of the channel width-to-depth (r_2) on the flow velocity distribution and the fluid energy loss on the cross-section of the flow[49,50]; therefore, it was included in further analysis processes.

The relationship among the physical variations (θ, r_1, r_2, L_{min}, v, ρ, n) that affect the fluid pressure Δp in the labyrinth channel was expressed as:

$$\varphi(\theta, r_1, S, r_2, L_{min}, v, \rho, n, \Delta p) = 0 \tag{10}$$

where, D, v, and ρ were selected as the basic quantities, six

independent π terms could be obtained using the dimensional analysis method and the π theorem as follows:

$$F(\theta, r_1, r_2, \frac{L_{min}}{S}, n, \frac{\Delta p}{v^2 \rho}) = 0 \tag{11}$$

Solving the pressure difference results in:

$$\frac{\Delta p}{\rho g} = F_1(\theta, r_1, r_2, \frac{L_{min}}{S}, n)\frac{v^2}{2g} \tag{12}$$

Let $\zeta = F_1(\theta, r_1, r_2, L_{min}/S, n)$; all structures of the flow channel units are the same, and the resistance coefficient of each channel (ζ) is the same, so the formula is as follows:

$$\bar{\zeta} = F_2(\theta, r_1, r_2, \frac{L_{min}}{S}) \times n \tag{13}$$

Let $\zeta = F_2(\theta, r_1, r_2, L_{min}/S)$; substituting the simulated values into Equation (3) and calculating the logarithmic and linear regression analysis, the regression results are shown in Table 5, and each regression index (θ, r_1, r_2, L_{min}/S) had a significant impact on the local head loss ($p<0.05$).　The relationship between ζ and the structure parameters is as follows:

$$\bar{\zeta} = e^{5.056}\theta^{0.338}r_1^{0.802}r_2^{-1.660}\left(\frac{L_{min}}{S}\right)^{2.726} \quad (r^2=0.746) \tag{14}$$

Furthermore,

$$\zeta = \frac{156.96 \times n \times \theta^{0.338}r_1^{0.802}L_{min}^{2.726}}{r_2^{1.660}S^{2.726}} \tag{15}$$

W	**1**	**0.970****	−0.007	−0.01	−0.237**	**0.146***	**0.979****	0.000	0.138*
D	**0.970****	**1**	0.008	0.014	−.230**	−0.098	**0.991****	0.000	0.156**
θ	−0.007	0.008	**1**	0.257**	−0.735**	−0.076	0.023	0.002	−0.595**
S	−0.01	0.014	0.257**	**1**	0.256**	−0.121*	0.038	0.003	−0.453**
r$_1$	−0.237**	−0.230**	−0.735**	0.256**	**1**	−0.039	−0.227**	0.001	0.129*
r$_2$	0.146*	−0.098	−0.076	−0.121*	−0.039	**1**	−0.036	0.000	−0.060
L$_{min}$	**0.979****	**0.991****	0.023	0.038	−0.227**	−0.036	**1**	0.000	0.135*
n	0.000	0.000	0.002	0.003	0.001	0.000	0.000	**1**	0.288**
ζ	0.138*	0.156**	−0.595**	−0.453**	0.129*	−0.060	0.135*	0.288**	**1**
	W	D	θ	S	r$_1$	r$_2$	L$_{min}$	n	ζ

Note: 1. W, channel width, m; 2. D, channel depth, m; 3. θ, tooth tip angle; 4. S, tooth spacing, m; 5. r_1, the ratio of the tooth height-to-channel width; 6. r_2, the ratio of the channel width-to-depth; 7. L_{min}, the minimum value of the width and height; 8. n, the number of channel units; 9. ζ, Local resistance coefficient.

Figure 6　Correlation analysis of the structural resistance coefficient (ζ) and the structural parameters

Table 5　Summary information for the regression parameters

Model	Unstandardized coefficient		Standardized coefficient	T	p
	β	Standard error	Beta		
(constant)	5.056	0.216		23.452	0.000
θ	0.338	0.121	0.262	2.798	0.005
R$_1$	0.802	0.073	1.041	10.923	0.000
r$_2$	−1.660	0.746	−0.068	−2.226	0.027
L$_{min}$/D	2.726	0.202	0.790	13.520	0.000

(2) Local resistance coefficient (ζ) and structural resistance coefficient (Cs)

To facilitate comparisons and applications, the local resistance coefficient (ζ) was transformed according to Equation (9) to obtain the structural resistance coefficient (Cs), so that the value range of Cs is between 0 and 1.　Considering the correlation between the local resistance coefficient ζ of E1-E7 and the Dra, the regression analysis of the Cs and Dra was carried out.　Results show (Figure 7) that there was a good linear relationship between the Dra and Cs, indicating that we can represent the anti-clogging ability of

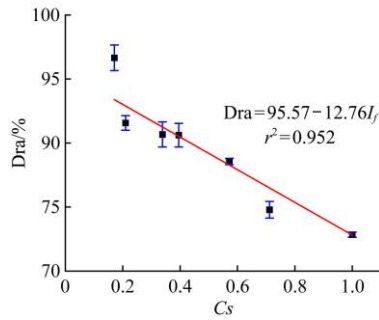different emitters.   The increase in Cs often means that the emitter had a reduced anti-clogging ability.

Figure 7   Linear regression analysis for the relative flow rate (Dra) - the structural resistance coefficient (Cs) for seven emitters (E1, E2, E3, E4, E5, E6, and E7)

3.3 Verification and application of the anti-clogging evaluation method

3.3.1   Reliability verification

As shown in Figure 8, by comparing the fitting coefficients with three structural coefficients at the end of the irrigation treatment and the Dra, it was shown that Cs responded more comprehensively and sensitively to changes in the anti-clogging ability caused by variations in the structural parameters than the two other structural coefficients[51-53].   The most plausible explanation may be that it comprehensively considers the structural characteristics of the labyrinth channel (Figure 8).   Based on its good linear relationship, Cs comprehensively links the structural characteristics of the emitter with the clogging characteristics by expressing the flow field changes and the energy conversion and dissipation characteristics.   It can effectively indicate the anti-clogging ability of the emitter.
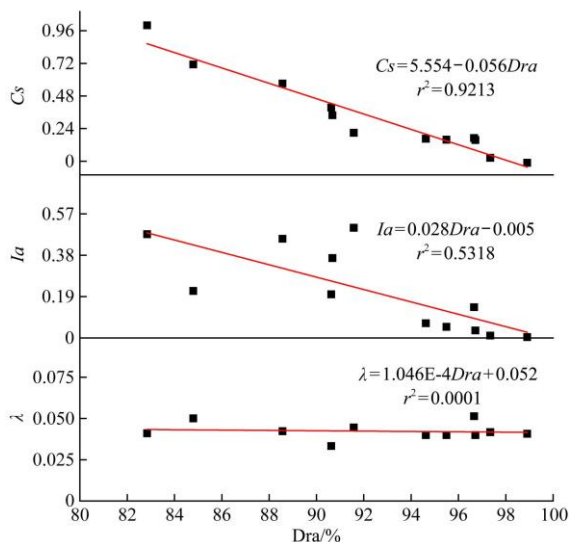
Note: Ia and λ mean two other structural coefficients proposed by Zhou and Wen et al.[51-53].

Figure 8   Response of the structural coefficients (Cs) to the emitter clogging (Dra)

3.3.2   Application

The fluidity index (x) reflects the turbulence of the fluid in the labyrinth channel to a certain extent.   As shown in Figure 9, the flow regime index (x) decreased with the increase of Cs, and a significant power function relationship was shown between them.   By considering the energy dissipation and irrigation uniformity, the lower the flow regime index (x), the better; but to reduce emitter clogging, the drip irrigation system requires emitters with smaller

Cs.   Regression analysis results revealed a negative correlation between the two indexes.   Therefore, the flow regime index (x) and Cs provide a set of conflicting parameters for developing drip irrigation systems.   An optimized combination for these parameters is required to yield irrigation uniformity and good anti-clogging performances.   In practice, an emitter with a flow regime index (x) less than 0.425 has an extremely high process and equipment investment requirements, so the production of this emitter is not realistic; however, if the flow regime index (x) is larger than 0.5, the energy dissipation effect of the emitter does not meet the energy dissipation requirements.   Thus, considering that the flow regime index (x) of a suitable drip irrigation system ranges within 0.425-0.475, it can be seen from Figure 9 that the value of Cs is between 0.146-0.461, and the emitter with a Cs within this range would be optimal.
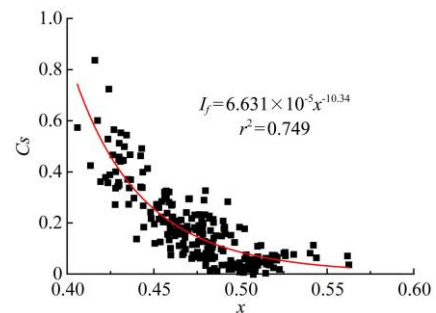

Figure 9   Fitting diagram of Cs-x of simulating emitters

Therefore, for the already manufactured emitters, Cs as an intermediate variable could help explore the relationship between the structural characteristics and the degree of emitter clogging, which is of great significance for the operability of emitter clogging risk assessment.   The goal of the optimal design of the emitter structure is to keep the smallest possible turbulent area where suspended matter deposition may occur based on maintaining the maximum pressure drop.   Furthermore, the optimization process should comprehensively consider the influence of structural parameters on the flow regime index and Cs to optimize the hydraulic and anti-clogging performance of the irrigator.   It is expected that this scientific emitter anti-clogging evaluation and emitter selection guidelines will benefit the efficient operation of drip irrigation systems and the improvement of water use efficiency.   However, how to use the emitter structure resistance coefficients to divide and evaluate the anti-clogging abilities of different emitters requires further research.

4   Conclusions

1) The emitter's anti-clogging ability is seemingly independent of the irrigation water quality, operating pressure, flushing frequency, irrigation frequency, or testing methods, as it is attributed to the emitter itself.   The greater the structural resistance of the coefficient (Cs) of the emitter labyrinth channel structure, the worse the anti-clogging ability and the greater the risk of clogging.

2) The calculation formula, which considers the tooth tip angle (θ), tooth height/runner width (H/W), tooth spacing (S), minimum cross-sectional size (L_{min}), channel width-to-depth ratio (W/D), and channel unit number (n) as the main reference parameters, can more genuinely reflect the actual resistance conditions in the labyrinth channel.

3) There is a negative correlation between the flow regime index (x) and the structural resistance coefficient (Cs), and it is

necessary to optimize the combination of the two indexes to obtain an optimal energy dissipation and irrigation uniformity while maintaining the system's anti-clogging performance. In the practical production process, when considering that the flow regime index range of the suitable drip irrigation system is 0.425-0.475, it is preferable to install an emitter with a structural resistance coefficient (*Cs*) of 0.146-0.461 to improve the anti-clogging performance.

Acknowledgements

[References]

[1]　Utkhede R S. Influence of drip microjet and sprinkler irrigation systems on the severity of crown and root of M. 26 apple rootstock trees in clay soil. Australas Plant Path, 1999; 28: 254–259.

[2]　Benouniche M, Kuper M, Hammani A, Boesveld H. Making the user visible: analysing irrigation practices and farmers' logic to explain actual drip irrigation performance. Irri Sci, 2014; 32(6): 405–420.

[3]　Kachwaya D S, Chandel J S, Vikas G, Khachi B. Effect of drip and furrow irrigation on yield and physiological performance of strawberry (*Fragaria × ananassa* Duch.) cv. Chandler. Indian Journal of Plant Physiology, 2016; 21: 341–344.

[4]　Li H R, Mei X R, Wang J D, Huang F, Hao W P, Li B G. Drip fertigation significantly increased crop yield water productivity and nitrogen use efficiency with respect to traditional irrigation and fertilization practices: A meta-analysis in China. Agr Water Manage, 2021; 244: 106534. doi: 10.1016/j.agwat.2020.106534.

[5]　Mpanga I K, Idowu O J. A Decade of Irrigation Water use trends in Southwestern USA: The role of irrigation technology best management practices and outreach education programs. Agr Water Manage, 2021; 243: 106438. doi: 10.1016/j.agwat.2020.106438.

[6]　Zhang T B, Zou Y F, Kisekka I, Biswas A, Cai H J. Comparison of different irrigation methods to synergistically improve maize's yield water productivity and economic benefits in an arid irrigation area. Agr Water Manage, 2021; 243: 106497. doi: 10.1016/j.agwat.2020.106497.

[7]　Oron G, DeMalach J, Hoffman Z, Cibotaru R. Subsurface microirrigation with effluent. J Irrig Drain Eng, 1991; 1: 25–36.

[8]　Barragan J, Cots L, Monserrat J, Lopez R, Wu I P. Water distribution uniformity and scheduling in micro-irrigation systems for water saving and environmental protection. Biosyst. Eng, 2010; 107(3): 202–211.

[9]　Wang Z, Li J, Li Y. Effects of drip irrigation system uniformity and nitrogen applied on deep percolation and nitrate leaching during growing seasons of spring maize in semi-humid region. Irri Sci, 2014; 32: 221–236.

[10]　Pérez-Ortolá M, Daccache A, Hess T M, Knox J W. Simulating impacts of irrigation heterogeneity on onion (*Allium cepa* L.) yield in a humid climate. Irri Sci, 2015; 33: 1–14.

[11]　Guan H J, Li J S, Li Y K. The synergistic effects of drip system uniformity and soil variability on drainage and nitrate leaching under arid conditions: A numerical study. Irrig Drain, 2019; 68: 950–960.

[12]　Contreras J I, Baeza R, Alonso F, Cánovas G, Gavilán P, Lozano D. Effect of distribution uniformity and fertigation volume on the bio-productivity of the greenhouse zucchini crop. Water, 2020; 12(8): 2183. doi: 10.3390/w12082183

[13]　Li Y K, Liu Y Z, Li G B, Xu T W, Liu H S, Ren S M, et al. Surface topographic characteristics of suspended particulates in reclaimed wastewater and effects on clogging in labyrinth drip irrigation emitters. Irri Sci, 2012; 30: 43–56.

[14]　Niu W Q, Liu L. Influences of sediment concentration and water temperature of muddy water on emitter clogging. Transactions of the CSAM, 2012; 43: 39–45. (in Chinese)

[15]　Niu W Q, Liu L, Chen X. Influence of fine particle size and concentration on the clogging of labyrinth emitters. Irri Sci, 2013; 31: 545–555.

[16]　Feng D, Kang Y H, Wan S Q, Liu S P. Lateral flushing regime for managing emitter clogging under drip irrigation with saline groundwater. Irri Sci, 2017; 35(3): 217–225.

[17]　Zhang R C, Niu. W Q, Duan X H, Li Y. Optimization of drip irrigation uniformity model considering location of clogged emitters. Transactions of the CSAE, 2017; 33: 113–120. (in Chinese)

[18]　Han S Q, Li Y K, Zhou B, Liu Z Y, Feng J, Xiao Y. An in-situ accelerated experimental testing method for drip irrigation emitter clogging with inferior water. Agr Water Manage, 2019; 212: 136–154.

[19]　Zhang J, Zhao W H, Tang Y P, Wei Z Y, Lu B H. Numerical investigation of the clogging mechanism in labyrinth channel of the emitter. Int. J Numer Meth Eng, 2007; 70: 1598–1612.

[20]　Wei Q S, Lu G, Liu J, Shi Y S, Dong W C, Huang S H. Evaluations of emitter clogging in drip irrigation by two-phase flow simulations and laboratory experiments. Comput Electron Agr, 2008; 63: 294–303.

[21]　Feng J, Wang W N, Liu H S. Study on fluid movement characteristics inside the emitter flow path of drip irrigation system using the Yellow River water. Sustainability-Basel, 2020; 12(4): 1319. doi: 10.3390/su12041319.

[22]　Liu H S, Li Y, Liu Y K, Yang P L, Ren S M, Wei R J, et al. Flow Characteristics in Energy Dissipation Units of Labyrinth Path in the Drip Irrigation Emitters with DPIV Technology. J Hydrodyn, 2010; 22: 137–145.

[23]　Li Y, Yang P L, Xu T W, Ren S M, Lin X C, Wei R J, Xu H B. CFD and digital particle tracking to assess flow characteristics in the labyrinth flow path of a drip irrigation emitter. Irri Sci, 2008; 26: 427–438.

[24]　Wu D, Li Y, Liu H S, Yang P L, Sun H S, Liu Y Z. Simulation of the flow characteristics of a drip irrigation emitter with large eddy methods. Math Comput Model, 2013; 58: 497–506.

[25]　Al-Muhammad J, Tomas S, Anselmet F. Modeling a weak turbulent flow in a narrow and wavy channel: case of micro-irrigation. Irri Sci, 2016; 34(5): 361–377.

[26]　Ge L X, Wei Z Y, Cao M, Tang Y P, Lu B H. Deposition law of sand in labyrinth-channel of emitter. Transactions of the CSAE, 2010; 26: 20–24. (in Chinese)

[27]　Yu L M, Li N, Long J, Liu X G, Yang Q L. The mechanism of emitter clogging analyzed by CFD-DEM simulation and PTV experiment. Adv Mech Eng, 2018; 10(1): 1–10. doi: 10.1177/1687814017743025.

[28]　Yan D Z, Yang P L, Ren S M. Study on dynamic analysis of particle movement in drip emitter based on CFD. Transactions of the CSAM, 2007; 38(6): 71–74, 81. (in Chinese)

[29]　Bucks D A, Nakayama F S, Gilbert R G. Trickle irrigation water quality and preventive maintenance. Agr Water Manage, 1979; 2(2): 149–162.

[30]　Duran-Ros M, Puig-Barguós J, Arbat G, Barragán J, Cartagena F R D. Effect of filter emitter and location on clogging when using effluents. Agr Water Manage, 2009; 96(1): 67–79.

[31]　Adin A, Sacks M. Dripper-clogging factors in wastewater irrigation. J Irrig Drainage Eng-ASCE, 1991; 117(6): 813–826.

[32]　Zhang J, Zhao W H, Tang Y P, Lu B H. Structural optimization of labyrinth-channel emitters based on hydraulic and anti-clogging performances. Irri Sci, 2011; 29: 351–357.

[33]　Yu L M, Li N, Yang Q L, Liu X G. Influence of flushing pressure before irrigation on the anti-clogging performance of labyrinth channel emitters. Irrig Drain, 2018; 67(2): 191–198.

[34]　Feng J, Li Y K, Wang W N, Xue S. Effect of optimization forms of flow path on emitter hydraulic and anti-clogging performance in drip irrigation system. Irri Sci, 2018; 36(1): 37–47.

[35]　Zhang L, Wu P T, Zhu D L, Zheng C. Effect of pulsating pressure on labyrinth emitter clogging. Irri Sci, 2017; 35: 267–274.

[36]　Wei Z Y, Cao M, Liu X, Tang Y P, Lu B H. Flow behaviour analysis and experimental investigation for emitter micro-channels. Chinese Journal of Mechanical Engineering, 2012; 25: 729–737.

[37]　Yang B, Wang J D, Zhang Y Q, Wang H T, Ma X P, Mo Y. Anti-clogging performance optimization for dentiform labyrinth emitters. Irri Sci, 2020; 38: 275–285.

[38]　Anderson J D. Computational fluid dynamics: the basics with applications, 1995; McGraw-Hill, New York.

[39]　Li Y K. Design of fractal flow path for emitters and experiment study and modeling on its fluid mechanism. China Agricultural University, 2005; 140p. (in Chinese)

[40]　Zhou B, Wang D, Wang T Z, Li Y K. Chemical clogging behavior in drip irrigation systems using reclaimed water. Transactions of the ASABE, 2018; 61: 1667–1675.

[41] Yang X Q, Wang Z, Liu H Q, Li J S. Effect of Phosphorus and Nitrogen Fertigation on Clogging in Drip Emitters Applying Saline Water. Journal of Irrigation and Drainage, 2020; 39: 68–76. (in Chinese)

[42] Liu Y F. Characteristics and mechanism of emitter clogging in drip irrigation with hard water. Northwest A&F University, 2018. (in Chinese)

[43] Li Q, Song P, Zhou B, Xiao Y, Muhammad T, Liu Z Y, et al. Mechanism of intermittent fluctuated water pressure on emitter clogging substances formation in drip irrigation system utilizing high sediment water. Agr Water Manage, 2019; 215: 16–24.

[44] Liu Z Y, Xiao Y, Li Y K, Zhou B, Feng J, Han S Q, Muhammad T. Influence of operating pressure on emitter anti-clogging performance of drip irrigation system with high-sediment water. Agr Water Manage, 2019; 213:174–184.

[45] Zhou H X, Li Y K, Wang Y, Zhou B, Bhattarai R. Composite fouling of drip emitters applying surface water with high sand concentration: Dynamic variation and formation mechanism. Agr Water Manage, 2019; 215: 25–43.

[46] Han S Q, Li Y K, Xu F P, Sun D X, Feng J, Liu Z Y, et al. Effect of lateral flushing on emitter clogging under drip irrigation with Yellow River water and a suitable method. Irrig Drain, 2018; 67: 199–209.

[47] Pei Y T, Li Y K, Liu Y, Zhou B, Shi Z, Jiang Y G. Eight emitters clogging characteristics and its suitability under on-site reclaimed water drip irrigation. Irri Sci, 2014; 32: 141–157.

[48] Wen G F. Study on effects of structure parameters of flow channel on hydraulic performance of drip emitters. Master dissertation. Yangling: Northwest A&F University, 2009; 55p. (in Chinese)

[49] Hui Y J, Hu C H. Effects of aspect ratio and sidewall roughness on velocity distribution and resistance coefficient in rectangular open channel. Advances in Water Science, 1991; 1: 22–31. (in Chinese)

[50] Tan X W, Wang Z Z, Zhao Y F, Zhao C L, Gao G. Study on Velocity Profile of Turbulent Fluid in Narrow Deep Type Rectangular Channel. Journal of Sichuan University (Engineering Science Edition), 2013; 45: 67–73. (in Chinese)

[51] Zhou B, Li Y K, Song P, Zhou Y P, Yu Y, Bralts V. Anti-clogging evaluation for drip irrigation emitters using reclaimed water. Irri Sci, 2017; 35: 181–192.

[52] Wen S L, Niu W Q, Wu M L, Zhang W Q, Li X K, Yang X K. Dynamic Characteristics of Different Emitters Clogging in Drip Irrigation with Muddy Water. Transactions of the CSAM, 2020; 51: 287–294. (in Chinese)

[53] Zhou B. Characteristics evaluation and mechanism of bio-clogging process in drip irrigation emitters. Doctoral dissertation. Beijing: China Agricultural University, 2016; 128p. (in Chinese)